Charge-State Dependent Compaction and Dissociation of Protein Complexes: Insights from Ion Mobility and Molecular Dynamics

Supporting Information

Zoe Hall[†], Argyris Politis[†], Matthew F. Bush[†,‡], Lorna J. Smith[§], Carol V. Robinson*[,†]

[†]Department of Chemistry, University of Oxford, Physical and Theoretical Chemistry Laboratory, South Parks Road, Oxford OX1 3QZ, United Kingdom

[§]Department of Chemistry, University of Oxford, Inorganic Chemistry Laboratory, South Parks Road, Oxford OX1 3QR, United Kingdom

[‡]Current Address: Department of Chemistry, University of Washington, Seattle, WA 98195, United States

*To whom correspondence should be addressed:

Tel: +44 1865 275473; Fax: +44 1865 275410; E-mail: carol.robinson@chem.ox.ac.uk

Supplementary Experimental Procedures

X-ray crystal structure calculations

Many computational methods are available to detect internal pockets and cavities in proteins[1-3]. The volumes of the cavities of the complexes were estimated using the Roll algorithm[4], implemented in POCASA (rolling sphere probe radius 1 Å, grid size 1 Å) freely available at http://altair.sci.hokudai.ac.jp/g6/service/pocasa/. The cavity volume was reported as a percentage of the solvent excluded volume of the complex. The program MSMS[5] was used to calculate the solvent-accessible surface areas, and volumes, of the protein complexes, with a probe radius of 1.4 Å. Gap volume index was calculated using SURFNET[6] on http://www.biochem.ucl.ac.uk. Structures were visualised using the molecular graphics program VMD[7].

Charge assignment algorithm

In order to assign charges to the protein complex, we first identified the solvent accessible basic residues. These were defined as Lys, Arg, and His residues that were <5 Å from the surface. The depth of residues was calculated using http://mspc.bii.a-star.edu.sg/tankp/[8]. In order to minimise coulombic repulsion, and attain an approximately even distribution of charges, we made use of an A* search algorithm[9]. This algorithm finds the least-cost path between points, called nodes, using a heuristic function to determine the order in which the search visits nodes in the tree. In this case, the nodes represented the solvent-accessible basic residues, and the least-cost path was that which minimised coulombic repulsion, by maximising the sum of distances between charged residues.

RMSD-clustering

In order to identify the most populated conformations at different stages in trajectories, we made use of an RMSD-clustering algorithm, based on the method of Daura *et. al.*[10] The general clustering approach is as follows: for each structure in the trajectory the backbone RMSD of the pentamer, relative to the starting structure at 0 ns, was calculated. Structures were grouped according to their RMSD, and those with RMSD within 0.1 nm of each other were considered to belong to a single cluster. Coordinates were written for the central structure of each cluster.

Supplementary Tables and Figures

Table S1. Degree of compaction observed in simulations and experiments for low, intermediate and high charge states of SAP

Charge state	MD simulations CCS_{calc} ($\mathring{A}^2$)		MD simulations $^a\Delta CCS_{calc}$ (%)	Experimental $^b\Delta CCS_{IM}$ (%)
18+	Initial	6828 ± 62	-7.3 ± 1.3 %	-10.2 ± 0.6 %
	Minimum	6328 ± 93		
25+	Initial	6882 ± 44	-3.0 ± 1.6 %	-0.2 ± 0.2 %
	Minimum	6677 ± 118		
30+	Initial	6946 ± 45	-1.0 ± 0.5 %	N/A
	Minimum	6875 ± 60		

$^a\Delta CCS_{calc}$ is the % difference between initial and minimum CCS for nine MD simulations with a linear temperature gradient.

$^b\Delta CCS_{IM}$ is the % difference between initial and minimum CCS observed in 3 repeat IM-MS experiments with increasing activation energy.
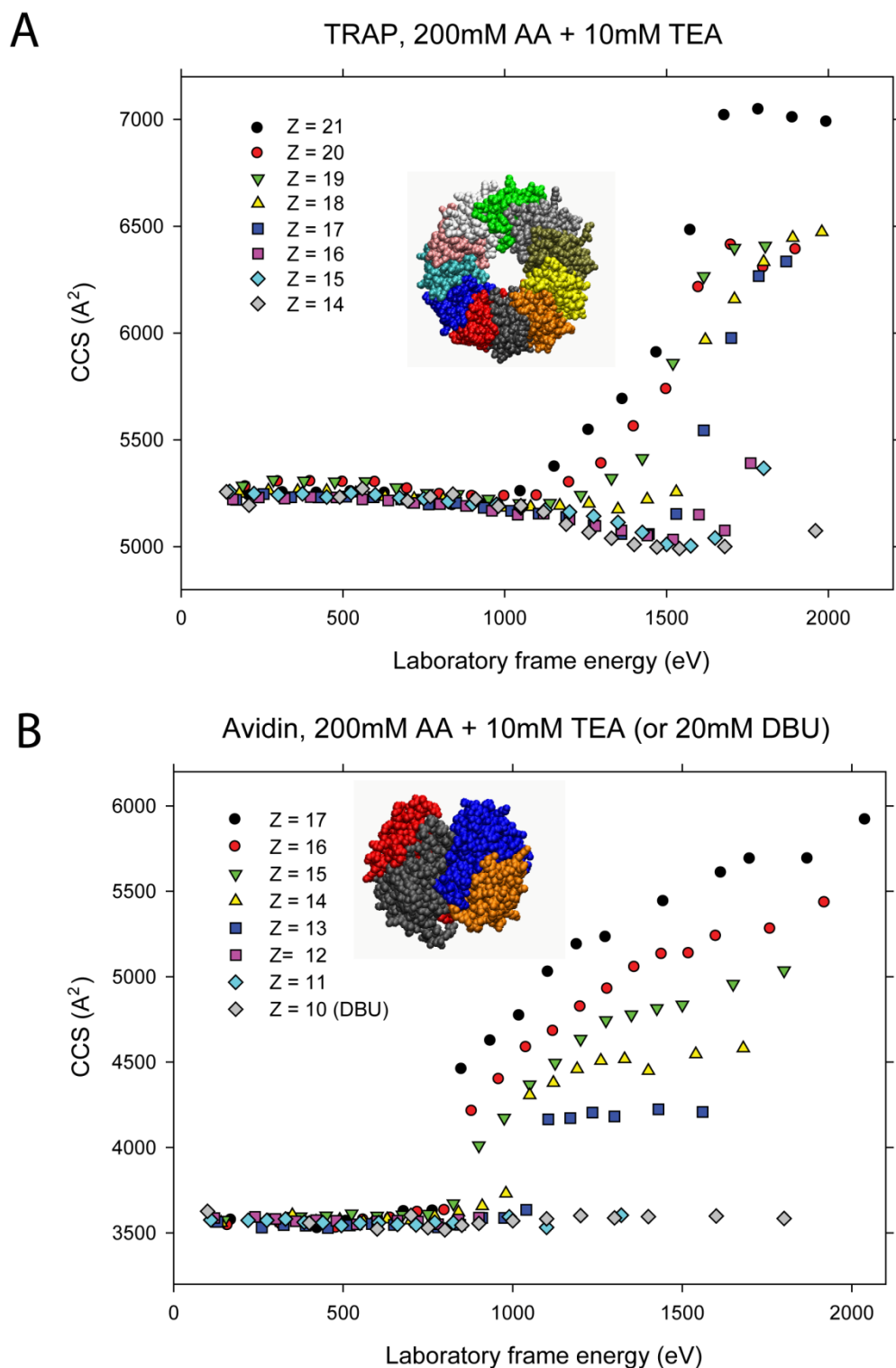
Figure S1. Unfolding pathways for additional protein complexes. The CCS of a wide range of charge states for TRAP (**A**) and avidin (**B**) was monitored using ion mobility, whilst increasing the laboratory frame energy (accelerating voltage x charge state). Strong charge state dependence was observed for the unfolding of each protein complex.
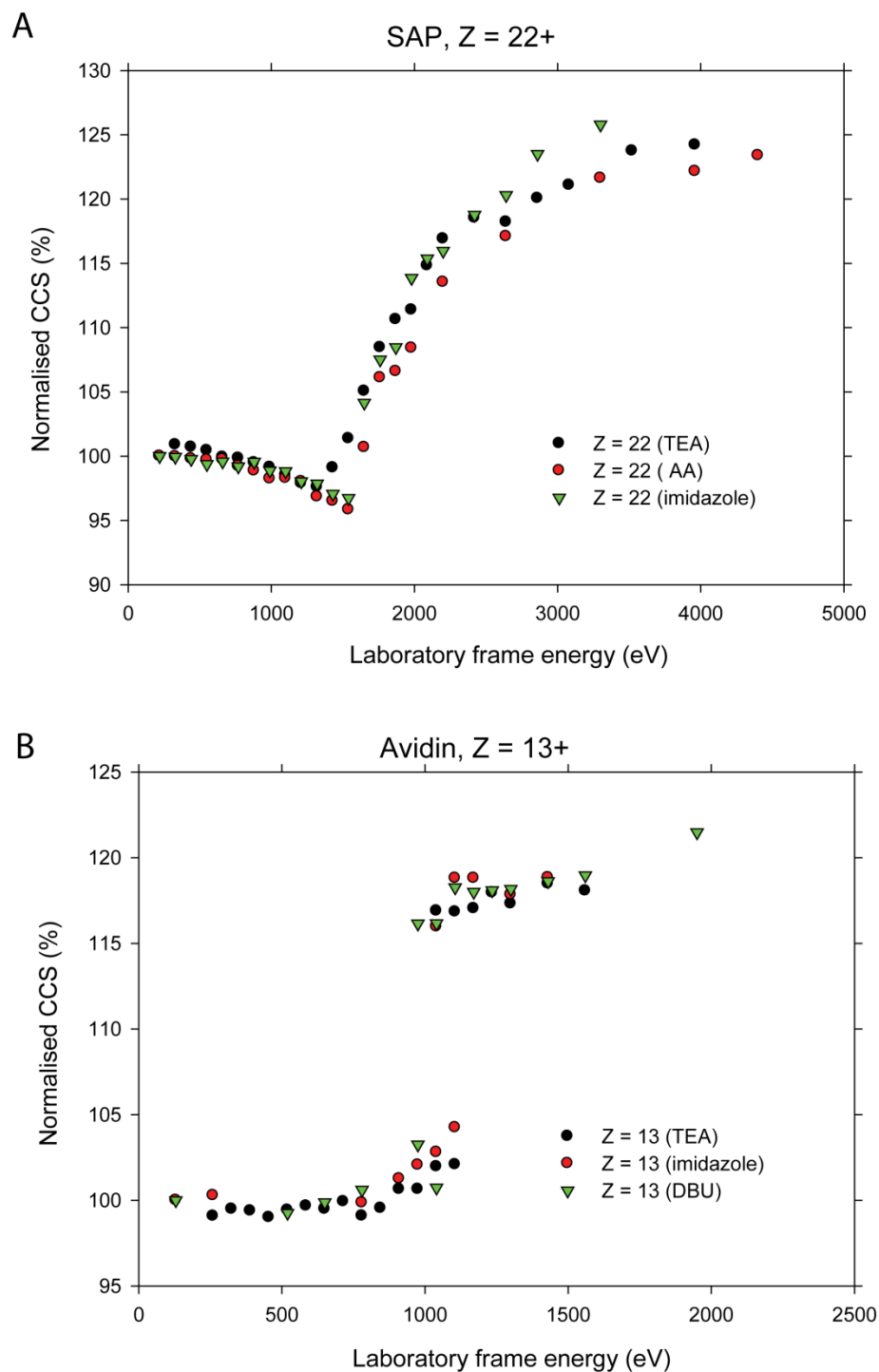
Figure S2. Evaluating the effect of the charge reducing agent on gas-phase unfolding of ions. The CCS of ions from different solution conditions were monitored over increasing laboratory frame energy. **A** SAP 22+ in 200mM AA with 10mM TEA (black), 10 mM imidazole (green) and 200 mM AA only (red). **B** Avidin 13+ in 200 mM ammonium acetate with 10 mM imidazole (red), 10 mM TEA (black), 20 mM DBU (green). Overall trends were not influenced by the presence or the type of charge reductant.
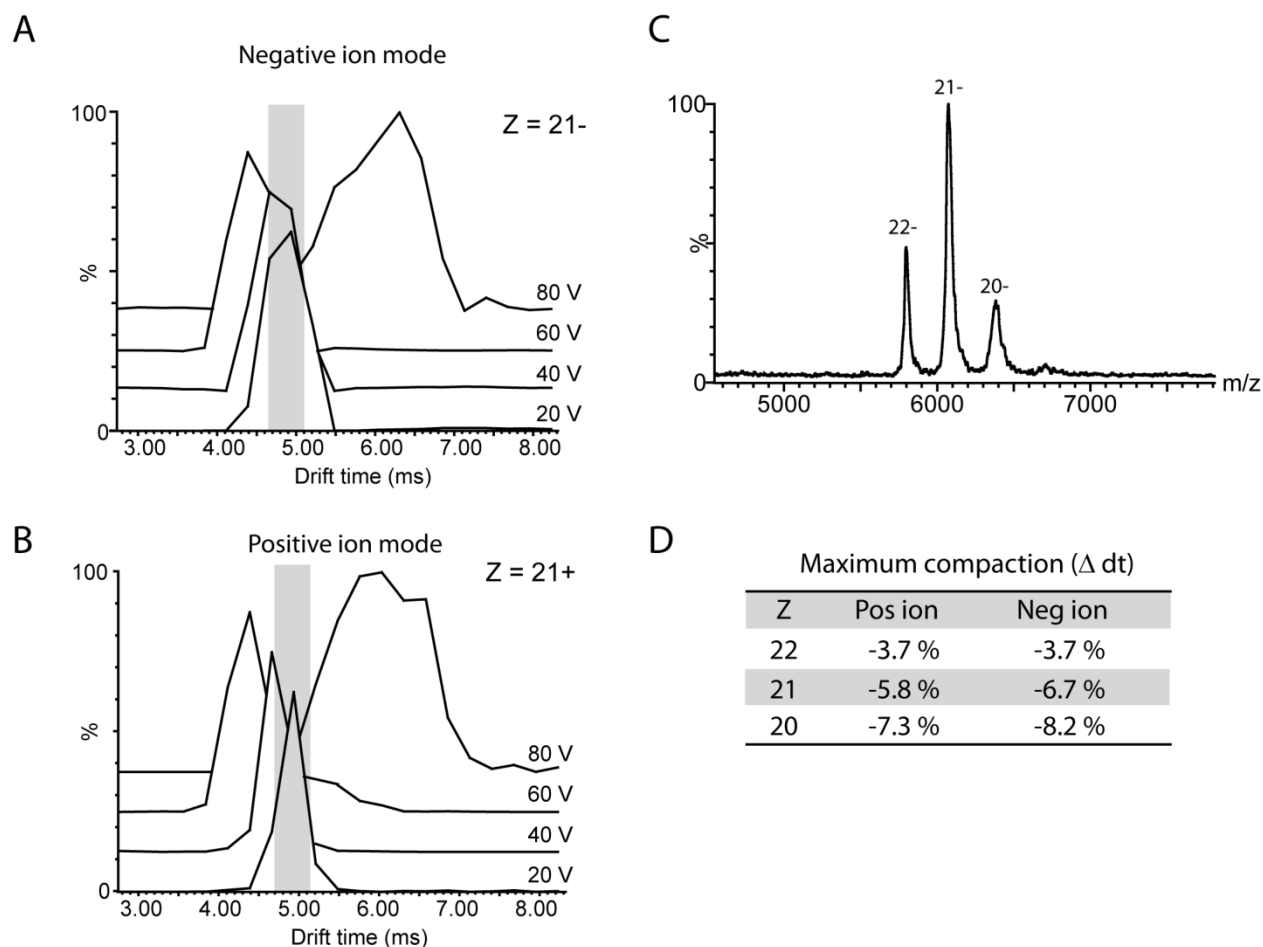
A Negative ion mode (Z = 21-)

B Positive ion mode (Z = 21+)

C MS spectrum, negative ion mode

D Maximum compaction (Δ dt)

Z	Pos ion	Neg ion
22	-3.7 %	-3.7 %
21	-5.8 %	-6.7 %
20	-7.3 %	-8.2 %

Figure S3. Negative ion mode was used in order to investigate whether similar conformational changes during collisional activation, which were observed for SAP in positive ion mode, could be detected. Drift time traces over increasing collision energies for SAP 21- in negative ion mode (**A**) and SAP 21+ in positive ion mode (**B**) are shown, and the MS spectrum for SAP in negative ion mode is shown in **C**. Due to the lower signal to noise encountered in negative ion mode, the Synapt HDMS G2 was used for this experiment. This travelling-wave type instrument cannot provide direct CCS measurements and requires CCS calibration. CCS values for large protein complex calibrants, however, are not available in negative ion mode, and thus to avoid introducing error we compare the changes in drift time for the two ion modes. Similar trends and extent of compaction were observed in both ion modes (**D**).
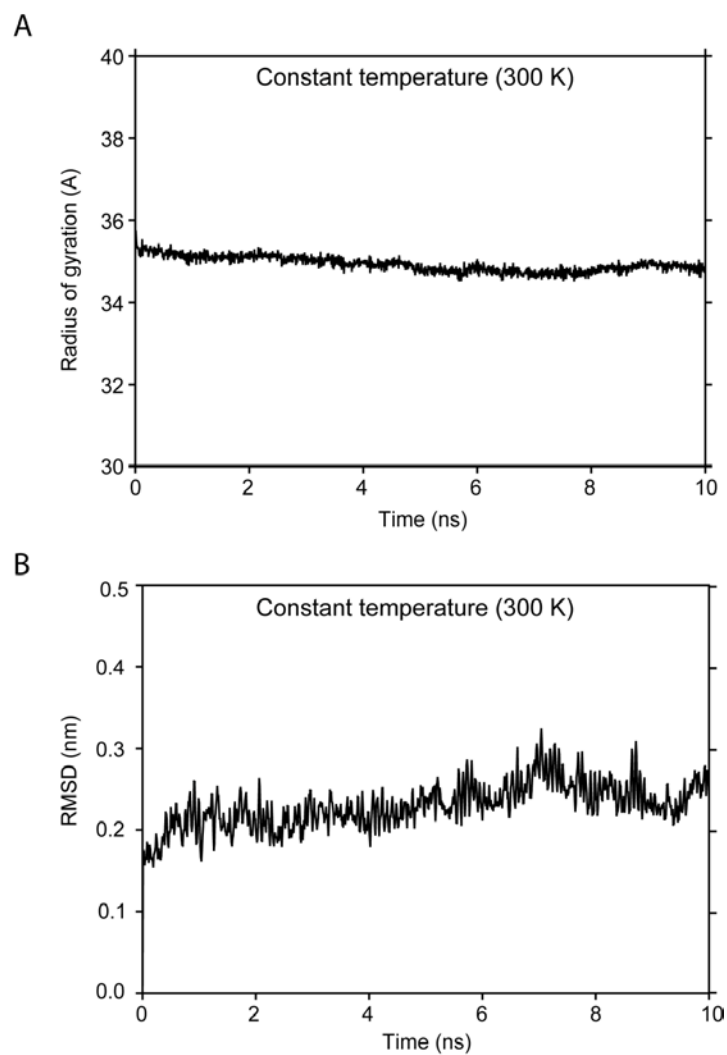
A

B

Figure S4. MD simulations of SAP *in vacuo* at constant temperature (300 K). A Radius of gyration for SAP 18+ over 10 ns simulations at constant temperature (300 K). **B** Backbone RMSD of the SAP 18+ pentamer, from the starting structure at 0 ns, over 10 ns simulations at constant temperature (300 K).
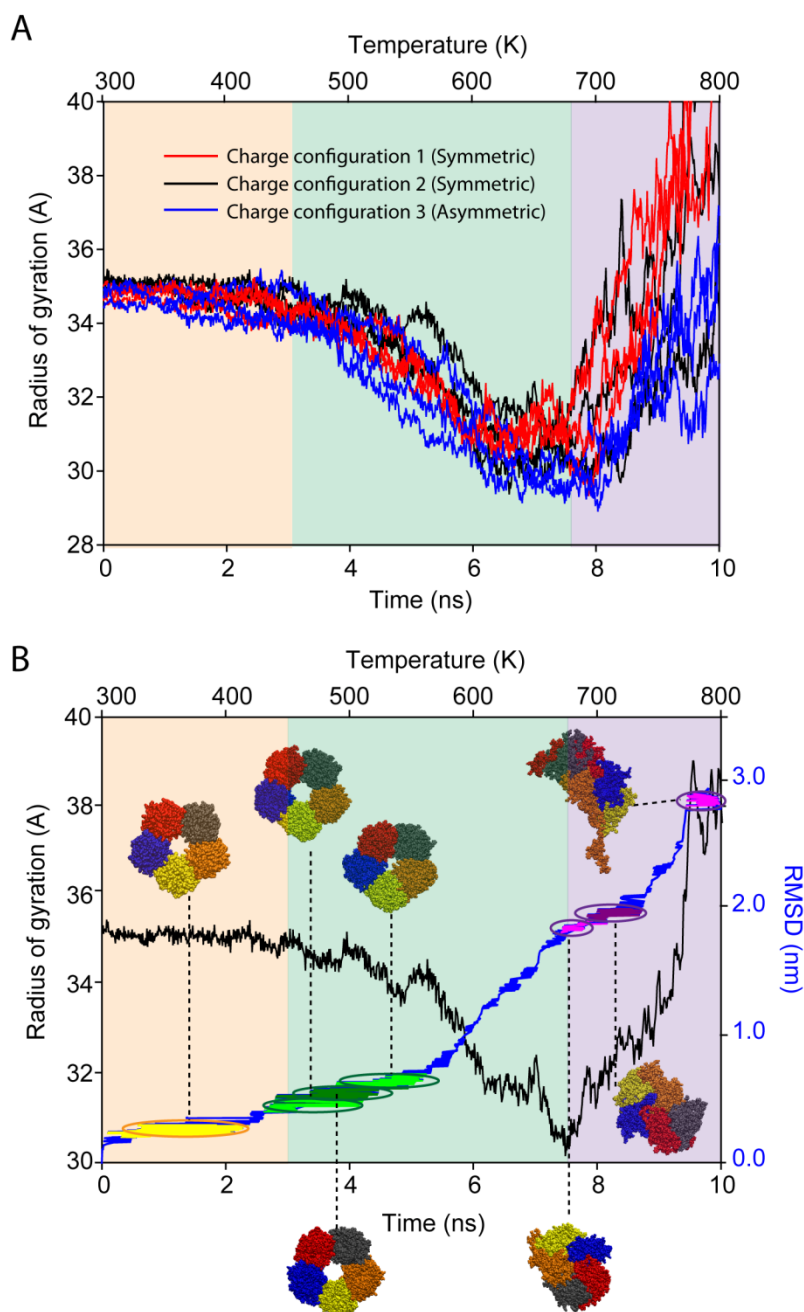
Figure S5. Analysis of *in vacuo* molecular dynamics simulations of SAP 18+. **A** Radius of gyration over 10 ns MD simulations with a linear temperature gradient (300 – 800 K), is shown for nine trajectories of SAP 18+. The three different charge configurations are shown in red, black and blue. Different regions were identified as constant R_g (~0–3 ns, yellow), decreasing R_g (~3–7.5 ns, green) and increasing R_g (~7.5–10 ns, purple). **B** The R_g and the backbone RMSD of the pentamer from the starting structure at 0 ns are shown, for a representative trajectory of SAP 18+, in black and blue respectively. RMSD clustering was performed as described and the most populated clusters in the three regions were identified (coloured yellow, green and purple). The central structure of each of these clusters is shown.
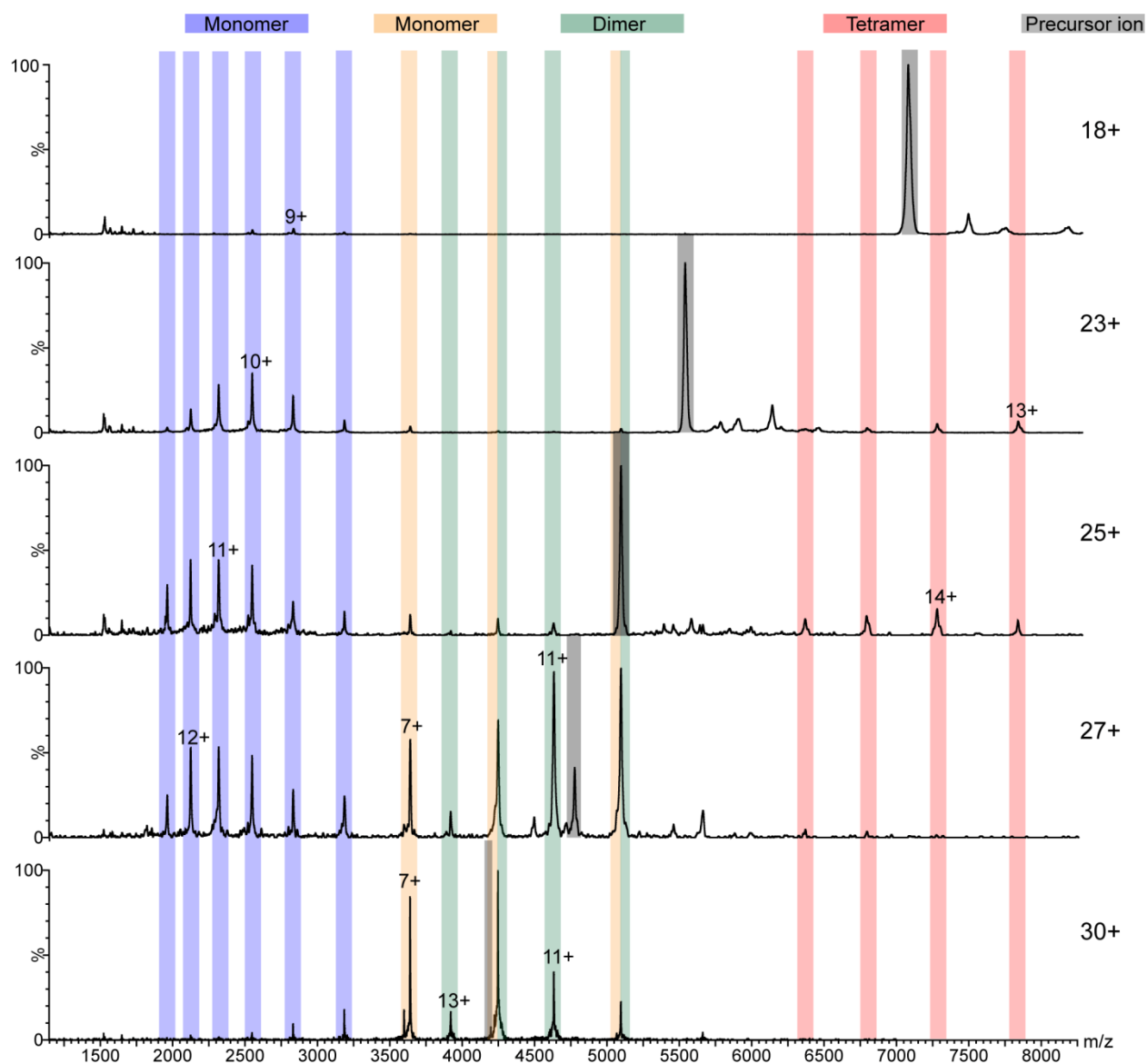
Figure S6. Charge-state dependent dissociation of SAP. MS/MS spectra are shown for selected charge states of SAP 5-mer at similar laboratory frame energies (collision energy x Z). There is a shift from typical CID, with the loss of a highly charged monomer, to an atypical CID pathway, where compact dimers and monomers are dissociated from the intact complex. The atypical CID pathway becomes more prevalent as the charge state of the precursor ion increases.

Supplementary References

(1)   Sonavane, S.; Chakrabarti, P. *Plos Comp. Biol.* **2008**, *4*, 1.

(2)   Voss, N. R.; Gerstein, M. *Nucleic Acids Res.* **2010**, *38*, W555.

(3)   Till, M. S.; Ullmann, G. M. *J. Mol. Model* **2010**, *16*, 419.

(4)   Yu, J.; Zhou, Y.; Tanaka, I.; Yao, M. *Bioinformatics* **2010**, *26*, 46.

(5)   Sanner, M. F.; Olson, A. J.; Spehner, J. C. *Biopolymers* **1996**, *38*, 305.

(6)   Laskowski, R. A. *J. Mol. Graphics* **1995**, *13*, 323.

(7)   Humphrey, W.; Dalke, A.; Schulten, K. *J. Mol. Graphics* **1996**, *14*, 33.

(8)   Chakravarty, S.; Varadarajan, R. *Structure* **1999**, *7*, 723.

(9)   Hart, P. E.; Nilsson, N. J.; Raphael, B. *IEEE Trans. Syst. Sci. Cybern.* **1968**, *4*, 100.

(10)   Daura, X., Gademan, K., Jaun, B., Seebach, D., van Gunsteren, W.F., Mark, A.E., *Angew. Chem. Int. Ed.* **1999**, *38*, 236.